UNIVERSITY OF CAMBRIDGE

Integrated fracture-based model formulation for RC crack analysis

Citation:

T.M. FAYYAD and J.M. LEES, Integrated fracture-based model formulation for RC crack analysis IN: ASCE Journal of Structural Engineering, *to appear*

Additional Information:

- Available online: tbc
- DOI: tbc

Version:

Accepted for publication

Please cite the published version.

Integrated fracture-based model formulation for RC crack analysis

Tahreer M. Fayyad[1] and Janet M. Lees[2]

[1] Former PhD Student, Department of Engineering, University of Cambridge, Trumpington Street, CB2 1PZ, Cambridge, United Kingdom, fayyadt@gmail.com

[2] Department of Engineering, University of Cambridge, Trumpington Street, CB2 1PZ, Cambridge, United Kingdom, jml2@eng.cam.ac.uk

T.M. FAYYAD and J.M. LEES, Integrated fracture-based model formulation for RC crack analysis IN: ASCE Journal of Structural Engineering, *to appear*

Abstract

There is an opportunity to revisit and generalise classical theories for concrete cracking in light of increased interest in the use of non-conventional reinforcing materials and material efficiency. Fracture-based models to describe concrete cracking have potential but a limitation has been that many variables and different phenomena have to be incorporated to produce realistic material models. In this paper, an integrated fracture-based model (IFBM) is developed to predict the behaviour of lightly reinforced concrete beams. The proposed model is a closed-form solution that integrates different local phenomena to more precisely describe the onset of cracking, crack propagation and crack rotation. The IFBM incorporates post-cracking tensile stresses in the concrete, the bond-slip behaviour between the reinforcement and concrete, and compression softening in the concrete compressive zone. The model can predict parameters such as the crack length development and crack mouth opening displacement in Mode I lightly reinforced concrete flexural specimens subjected to three-point bending. The predictions show a fairly good agreement with experimental results for small-scale reinforced concrete beams with low reinforcement ratios (0.15-0.5%). The ability of the IFBM to identify specific failure modes and to capture the crack propagation and crack rotation stages of behaviour in lightly reinforced concrete beams are particular advantages. Such an approach provides a powerful tool to study the problem of minimum reinforcement requirements.

Key words

Reinforced concrete, fracture, cracking, modelling, crack propagation

1. Introduction

Over the past decades various studies have investigated concrete cracking and the development of models to simulate the cracking process in reinforced concrete beams (Bazant and Kazemi 1990; Bažant and Oh 1983; Chan et al. 1993; Gerstle et al. 1992; Gerstle and Xie 1992; Gustafsson and Hillerborg 1988; Haskett et al. 2009a; Hillerborg et al. 1976; Jenq and Shah 1985; Karihaloo and Nallathambi 1989; Manfredi 1998; Mi et al. 2016; Ooi and Yang 2011; Paggi et al. 2009; Saleh and Aliabadi 1998). These models can broadly be classified as either plasticity-based models which are justified in the case of ductile behaviour e.g. beams with sufficient internal steel, or fracture mechanics-based models which do not treat fracture as a point phenomenon but use fracture mechanics principles to explain crack propagation. During fracture propagation the behaviour depends on what is happening in the fracture process zone (FPZ) ahead of the crack tip. This region is analytically challenging for model developers and structural engineers (Cedolin et al. 1983; Nomura et al. 1991; Ohno et al. 2014) because it is a transition zone between a discontinuous open crack and the continuous intact material beyond the crack. So it cannot be modelled using continuum variables (Bazant and Kim 1984; van Mier 1984). Although fracture mechanics provides the basis for a rational approach, and has been applied to concrete fracture problems for over forty years, it has typically not been widely adopted within design code equations. One contributing factor is that fracture mechanics approaches are often modelled using finite element tools and this presents difficulties in the development of general guidelines (van Mier 1995). Furthermore, civil engineers are less familiar with fracture mechanics formulations and the associated terminology. This means that conventional empirical stress-based approaches have been preferred for structural applications and total strain models are more common within current finite-element analyses.

Fracture in reinforced concrete involves diverse phenomena such as the formation of cracks, crack propagation, the existence of microcracks and interactions between the reinforcement and the concrete, and within the concrete e.g. cement and aggregate (Hillerborg et al. 1976). The presence of reinforcement in concrete affects the crack propagation and improves the fracture toughness. The concept of “crack bridging” emerged as a result of applying fracture mechanics models to reinforced concrete structures. The reinforcement bridges the crack opening and provides confinement to the

cracking process (Carpinteri and Massabo 1997). This confinement can increase the energy demand and be a source of size effects in reinforced concrete structures (Carpinteri and Massabo 1997; Nemati et al. 1998). Most theoretical models for RC fracture account for the reinforcement using the principle of superposition where the concrete fracture is considered in isolation and the effect of the reinforcement as a closing force is then added (Bosco and Carpinteri 1992; Carpinteri 1984; Carpinteri et al. 2007; Hillerborg 1990; Luchko 1996).

Fracture mechanics studies of concrete have often focused on mode I failures because, compared to other modes, mode I tests can be relatively easily conducted in laboratories (Jenq and Shah 1988) and can also provide insight for theoretical studies of shear failure (Carpinteri et al. 2007; Gastebled and May 2001; Jenq and Shah 1990; So and Karihaloo 1993). It has also been shown that the moment-rotation behaviour when there is a single hinge crack is either equal to or represents a lower bound to that which occurs when there are multiple crack hinges (Haskett et al. 2009a). The cracking mechanism associated with single crack propagation can therefore be extended to multiple cracks. This paper considers a single mode I flexural crack to develop the basis for an integrated fracture-based model that has both the potential for extension and scope for further validation to define the values of the controlling material parameters.

2. Literature review

A traditional analysis of a cracked reinforced concrete section is normally based on the assumption that under flexural loading plane sections remain plane. This approach does not consider the crack propagation process in detail. The effect of concrete in tension after cracking is also typically ignored. However, cracking in reinforced concrete is a sequential process that involves a gradual loss of tensile stresses with crack propagation. Studies have shown the existence of concrete softening in both tension and compression i.e. (Bažant et al. 1987; Crisfield 1982; Hillerborg 1990; Hillerborg et al. 1976) and this means that even in a cracked region, parts of the open crack still have some ability to transfer stress.

Linear elastic fracture mechanics (LEFM) was applied by Carpinteri when developing the Bridged Crack Model (BCM) to study the flexural failure of reinforced concrete beams (Carpinteri 1984) and to analyse shear cracks (Carpinteri et al. 2007). In the BCM model, it was assumed that when the crack

starts to grow, the resultant stress intensity factor equals the critical stress intensity factor K_{IC}. Deng and Matsumoto (2017) proposed an LEFM method to estimate the force in reinforcement crossing a crack in RC beams subjected to mode I loading. The bond slip at rebar-concrete interface was also taken into account. However, the use of LEFM is a limitation for a quasi-brittle material like concrete due to the existence of a considerable fracture process zone ahead of the crack tip. As LEFM is only valid when the size of the fracture process zone can be neglected, the Cohesive Crack Model (CCM) was proposed to model cracks in quasi-brittle materials taking into account the nonlinear behaviour in the fracture process zone (Griffith 1921). Hillerborg later applied the CCM to concrete using his Fictitious Crack Model (FCM) (Hillerborg et al. 1976). The difficulty in applying the FCM without a Finite Element framework led Gerstle et al. (1992) to simplify some assumptions related to the CCM to develop an analytical solution for flexural cracks in reinforced concrete beams. This model considered the concrete softening in tension; however, it did not consider the concrete compression softening or the bond-slip behaviour between concrete and steel (Gerstle et al. 1992). To investigate the mechanical behaviour of a crack in steel reinforced concrete, the behaviour of the steel was described using an elastic-plastic constitutive law and the bridging traction was deduced from the deformation of steel (Mi et al. 2016). Cohesive forces ahead of the crack tip were considered. The presence of cohesive forces implied that there was a relaxation of the stresses ahead of the crack tip where the stress intensity factor should be zero (as opposed to a stress concentration that can be expressed using the stress intensity factor *K*). However, in the solution *K* was considered and determined together with the cohesive forces (Mi et al. 2016). Numerical models based on LEFM and non-linear fracture mechanics (NLFM) can be used to simulate concrete cracking (Bažant and Oh 1983; Carpinteri 1984; Carpinteri et al. 2007; Gerstle et al. 1992; Hillerborg et al. 1976; Jenq and Shah 1985; Kaplan 1961; Ooi and Yang 2011). However, there are a lack of closed-form solutions which are preferable for implementation in standards and design codes. The proposed integrated fracture-based model reflects different local phenomena to more precisely describe the behaviour of reinforced concrete beams and provides an analytical solution for the development of flexural cracks in RC beams from the onset of cracking until failure. It incorporates post-cracking tensile stresses in the concrete, the bond-slip behaviour between the reinforcement and concrete, and compression softening in the concrete

compressive zone. In the following, the theoretical basis for the integrated RC cracking model and details of proposed model will be presented. The model predictions are benchmarked against selected experimental results on lightly reinforced concrete beams and existing analytical models.

3. Research significance and motivation

This research bridges the gap between a 'structural view' and a 'fracture view' of the cracking process in lightly reinforced concrete. The proposed fracture mechanics-based formulation is based on a closed-form solution rather than a finite element framework. This promotes the acceptance of fracture mechanics approaches within the structural concrete community and leads to a greater insight into structures that are sensitive to fracture. Fracture processes are particularly important for lightly reinforced concrete beams where the crack propagation and concrete tensile softening have a strong influence on the behaviour. An understanding of these phenomena will also inform a more fundamental definition of the minimum reinforcement requirements for reinforced concrete beams (Fayyad and Lees 2015). A further driver is that the input parameters in the fracture mechanics-based formulation are explicit so the model can be extended to describe lightly reinforced structures with non-conventional reinforcing materials such as advanced composites. This addresses a limitation with existing semi-empirical approaches for steel reinforced concrete which are not necessarily representative of structures with differing characteristics.

Reinforced concrete beams with low ratios of longitudinal reinforcement are the subject of the current work. A model is developed to investigate cracks in reinforced concrete and the effects of crack bridging due to the presence of longitudinal reinforcement. The developed predictive tool balances the need to reflect core material and geometric parameters that influence the behaviour with a desire for a tractable solution procedure. The model validation takes advantage of recent advances in image processing techniques where fracture properties were measured experimentally using three-point bending mode I lightly reinforced concrete beams (Fayyad and Lees 2017). The validation provides insight into the cracking process and the basis for comparison with predicted outputs such as the crack length development.

T.M. FAYYAD and J.M. LEES, Integrated fracture-based model formulation for RC crack analysis IN: ASCE Journal of Structural Engineering, *to appear*

4. Local phenomena in reinforced concrete

4.1 Tensile softening in concrete

Concrete has a low tensile strength when compared with its compressive strength. When the tensile strength is exceeded, micro-cracks appear in the tension zone and then quickly unite to form a macro-crack that propagates under loading. The propagation of the crack leads to softening in the concrete where the open crack still has a certain residual capability for stress-transfer due to interlocking and micro-cracking (Chen and Su 2013; Li et al. 1987). The incorporation of the tensile softening behaviour in predictive models has been found to lead to a more accurate and rational representation of cracking parameters and deflections (Gopalaratnam and Shah 1985). According to the FCM, the tension softening of concrete can be described by means of closing forces (stress) in the fracture process zone and a crack propagates when the stress at the crack tip σ reaches the concrete tensile strength f_t. When the crack opens, the stress σ decreases with increasing crack width w until it reaches zero stress at a critical width w_c. One of the simplest ways to reflect tensile softening is through the use of a linear softening curve (Figure 1(a)). Although a linear curve is a simplification, it can nevertheless provide an adequate description of the softening behaviour and the basis for closed form solutions. The associated cohesive forces (Figure 1(b)) are linear and decrease from a value of f_t at the point of zero crack opening to zero at a critical opening $w_c = C_r$. As the applied load increases, the crack opens and propagates but the crack still carries stresses that linearly decrease with the crack mouth opening displacement ($CMOD$). When $CMOD \leq C_r$ the total closing force, *CF*, per unit width acting along the crack length, *a*, is :

$$CF = \frac{1}{2}\, a\, (f_t + \left(1 - \frac{CMOD}{C_r}\right) f_t) = \frac{1}{2}\, a\, f_t \left(2 - \frac{CMOD}{C_r}\right) \quad (1)$$

When $CMOD = C_r$, the total closing force is $\frac{1}{2}\, a\, f_t$. As the crack propagates and the crack opening exceeds C_r at the crack mouth ($CMOD > C_r$), the total closing force becomes:

$$CF = \frac{1}{2}\, a\, f_t \left(\frac{C_r}{CMOD}\right) \quad (2)$$

4.2 Rotational capacity and compression softening in RC beams

The rotational capacity of an RC member can be defined as the ability to sustain post peak rotation. Post peak rotation is desirable because it allows for the optimum usage of the potential for moment redistribution after reinforcement yielding (Walraven 2007). The plastic rotational capacity depends on numerous parameters including the geometrical properties of the cross section, material properties, reinforcement type and ratio, interaction between the concrete and reinforcement and loading conditions (Bigaj and Walraven 2002; Kheyroddin and Naderpour 2007; Lopes and Bernardo 2003; Manfredi 1998). In lightly reinforced concrete beams with a very low reinforcement ratio, the fracture of the reinforcement limits the beam rotational capacity while with higher reinforcement ratios, a greater rotational capacity can be reached through concrete crushing in the compression zone (Walraven 2007). This means that firstly; the softening rotational capacity during the post-peak behaviour cannot be understood in isolation without considering what happens in the reinforcement and in the concrete progressively. Secondly, the softening of concrete in compression can affect the strength and ductility of RC members. Finally, the rotation capacity and compression softening are related and their effects are reciprocal.

Compressive strain softening is a complex behaviour (van Mier 1984; Watanabe et al. 2004). Most investigations have considered concrete under uniaxial compression (i.e. (Jansen and Shah 1997; Markeset and Hillerborg 1995; Shah and Sankar 1987; Torrenti et al. 1993; Watanabe et al. 2004)). The mechanical behaviour of reinforced concrete beams under strain localization has not been studied as extensively. Hillerborg developed a fracture mechanics-based model to study compression strain localization in reinforced concrete beams (Hillerborg 1990). He treated compression localization in a manner similar to that which occurs during tensile fracture. According to his model, the compression behaviour can be described by means of a stress-strain diagram ($\sigma_c - \varepsilon_c$) until the peak compressive strength is reached and thereafter using a stress-deformation diagram ($\sigma_c - w$) as shown in Figure 2(a). The localization was assumed to take place within a length proportional to the depth of the compression zone which changes with loading. van Vliet & van Mier also showed that the pre-peak behaviour could be described in terms of stress and strain (van Vliet and van Mier 1996). Jansen & Shah suggested that

the stress-deformation relationship is a material property that depends on the specimen size (Jansen and Shah 1997). Based on these conclusions, Carpinteri et al. (2009) developed an overlapping crack model where he referred to the deformation that occurs in compression after the peak stress as interpenetration. Instead of identifying a length where strain localization occurs, Carpinteri et al. (2009) assumed that strain localization develops progressively in the compression zone in a way that is similar to the generation of cohesive forces in the tension zone and hence a stress-deformation relationship similar to Hillerborg's was used. A numerical algorithm based on the finite element method was proposed (Carpinteri et al. 2009). Shear-friction theory has also been used to quantify the softening force in concrete subjected to compression (Haskett et al. 2009a; Oehlers et al. 2017). Borges et al. (2004) used a linear softening curve to study the uniaxial compressive response of concrete. A stress-deformation softening relationship was not included. Instead, the pre- and post-softening behaviours were defined using linear compressive stress, σ_c, versus strain, ε_c, relationships as shown in Figure 2(b). Knowledge of the compressive strength concrete, f_c, the critical damage strain, ε_{cr}, and the strain corresponding to the peak compressive strength, ε_0, are required. According to this softening curve:

$$\varepsilon_c = \varepsilon_{cr}\left(1 - \frac{\sigma_c}{f_c}\right) + \varepsilon_0\left(\frac{\sigma_c}{f_c}\right) \tag{3}$$

Non-linear stress-strain based softening curves have also been proposed e.g. (Hognestad et al. 1955; Thorenfeldt et al. 1987). When the strain varies through a compression zone, the corresponding force resultants are found by integration. In the current work, a linear relationship between the concrete compressive stress and strain was assumed to simplify the integration step so that the equations could be solved directly. This enables an analytical solution for flexural cracking while capturing features of the compressive softening behaviour. However, it is recognised that this is a simplification and the exploration of more complex softening models is the subject of further work.

4.3 Crack bridging

Bond between the internal reinforcement and concrete is required for reinforced concrete to act as a composite material and to ensure the transfer of load between the two materials. This interaction is represented in the literature as shear stresses τ at the reinforcement/concrete interface. The development

of bond stresses results in a relative displacement between the reinforcement and the concrete parallel to the reinforcement axis referred to as the slip, s. The bond-slip behaviour of reinforced concrete affects the crack opening and forms the basis for the calculation of the crack width and crack opening. Although the details of the bond stress-slip behaviour are complex, a mathematical relationship is required for modelling purposes. In a constant bond-stress slip model, the bond stress, τ, maintains a constant value that does not depend on the slip. However, this model does not represent the actual behaviour of reinforcement in concrete. More representative, albeit more complicated, bond-slip relationships have been proposed (Casanova et al. 2012; Elmorsi 2000; Focacci et al. 2000; Martin 1973; Mirza and Houde 1979; Rehm 1961). Most of the models were derived based on the 'curve-fitting' of experimental results. Some depend on experimental constants (Martin 1973; Rehm 1961). Others are higher order relationships (Mirza and Houde 1979) or designed for a finite element framework (Casanova et al. 2012; Elmorsi 2000; Focacci et al. 2000; Ingraffea et al. 1984) so are rather complicated for use in mechanics solutions or closed-form models. Eligehausen et al. (1982) suggested a nonlinear relationship with increasing τ and s when $0 \leq s \leq s_1$ until $\tau = \tau_{max}$ where

$$\tau(s) = \tau_{max} \left(\frac{s}{s_1}\right)^{\alpha} \tag{4}$$

Yuan et al. (2004) used a bi-linear approximation (see Figure 3) to study the bond interface between fibre reinforced polymers (FRPs) and concrete whereas Mohamed Ali et al. (2008) and Haskett et al. (2008) idealized the bi-linear relationship as a linear descending relationship (Figure 3). In this case, the bond-slip behaviour is defined by:

$$\tau(s) = \tau_{max} \left(1 - \frac{s}{s_{max}}\right) \tag{5}$$

where τ_{max} and s_{max} are determined experimentally and depend on the concrete and reinforcement properties.

4.3.1 Bridging force

The equilibrium conditions for a section of a reinforcing bar in tension and surrounded by concrete are shown in Figure 4. The slip ds between the reinforcement and the concrete over a length dx equals the

difference between the strain in the reinforcement, ε_s , and the concrete, ε_c. Incorporating the elastic constitutive laws for the two materials where $\sigma_s = E_s\varepsilon_s$, and $\sigma_c = E_c\varepsilon_c$ and differentiation with respect to x gives:

$$\frac{d^2s}{dx^2} = \frac{1}{E_s}\frac{d\sigma_s}{dx}\left(1 - \frac{E_s}{E_c}\frac{d\sigma_c}{d\sigma_s}\right) \tag{6}$$

The balance of longitudinal forces in the element dx and the reinforcement then leads to:

$$\frac{d^2s}{dx^2} = \frac{1}{E_s}\frac{d\sigma_s}{dx}\left(1 + \frac{A_s}{A_c}\frac{E_s}{E_c}\right) \tag{7}$$

and:

$$\frac{d\sigma_s}{dx} = \frac{\tau\,(s)L_{per}}{A_s} \tag{8}$$

where L_{per} is the contact perimeter of the reinforcement with the surrounding concrete.

Substituting $\frac{d\sigma_s}{dx}$ from equation (8) into equation (7) results in

$$\frac{d^2s}{dx^2} = \tau(s)\,L_{per}\left(\frac{1}{A_sE_s} + \frac{1}{A_cE_c}\right) \tag{9}$$

Equation (9) represents the general governing ordinary differential equation defining the bond behaviour between the concrete and the reinforcement. Its solution depends on the function that defines the bond stress-slip relationship $\tau(s)$ (Lees and Burgoyne 1999; Seracino et al. 2007; Wu and Zhao 2012; Wu et al. 2002).

4.3.2 Idealised linear bond relationships

For an idealized linear bond stress-slip relationship, equation (5) is substituted into equation (9) (and assuming that A_cE_c is large when compared with A_sE_s such that the $\frac{1}{A_cE_c}$ term can be ignored) to give:

$$\frac{d^2s}{dx^2} + \lambda^2\,s = \lambda^2 s_{max} \tag{10}$$

where λ^2 is defined as:

$$\lambda^2 = \frac{L_{per}}{A_s E_s} \frac{\tau_{max}}{s_{max}} \tag{11}$$

This equation is a second order non-homogenous differential equation that can be solved using the boundary conditions at $x = 0$, where both $s = 0$ and $\frac{ds}{dx} = 0$ and leads to:

$$s = s_{max}(1 - \cos \lambda x) \tag{12}$$

Combining equations (5), (8) and (12) and integrating with respect to x gives the reinforcement force P where:

$$P = \frac{\tau_{max}\, L_{per}}{\lambda} \sin \lambda x \tag{13}$$

The force P can also be expressed as a function of the slip s:

$$P = \frac{\tau_{max}\, L_{per}}{\lambda} \sin\left\{\arccos\left\{\frac{s_{max} - s}{s_{max}}\right\}\right\} \tag{14}$$

when the slip s at the crack face is less than s_{max}, and the overall length of a pull-out specimen, L , is sufficient to build up the necessary bond stresses (Figure 5(a)).

The axial force, P, will have a maximum value when the slip at the crack face reaches s_{max} and the shear stress is equal to zero (Figure 5(a)). The maximum force P_{max} therefore occurs when $\sin \lambda l = 1$ and l reaches a critical value l_{cr} where

$$l_{cr} = \frac{\pi}{2\,\lambda} = \frac{\pi}{2\sqrt{\frac{\tau_{max}\, L_{per}}{s_{max}\, A_s E_s}}} \tag{15}$$

However, if the specimen length L is not sufficient to develop l_{cr} (Figure 5(b)), then P_{max} cannot be achieved and the reinforcement force associated with debonding, P_d, is defined as:

$$P_d = \frac{\tau_{max}\, L_{per}}{\lambda} \sin \lambda L \tag{16}$$

T.M. FAYYAD and J.M. LEES, Integrated fracture-based model formulation for RC crack analysis IN: ASCE Journal of Structural Engineering, *to appear*

4.3.3 Strain hardening of steel and debonding - Haskett et al. approach

Haskett et al. developed a model that took into account the combined effects of steel strain hardening and the bond-stress slip behaviour in reinforced concrete. The assumed linear bond stress-slip distribution was defined for two stages (Haskett et al. 2009b). In the first stage the steel is elastic and defined by an elastic modulus E_s up until the point where the steel yields at a stress f_y and a strain ε_y. During the second stage, the steel has yielded and the stress-slip relationship changes according to the strain hardening modulus E_{sh} until fracture occurs at a stress, σ_{fract}, and a strain, ε_{fract}. The elastic and the strain hardening behaviours were then added together (Haskett et al. 2009b).

The elastic steel force SF_{el} was calculated using E_s such that (Figure 6(a))

$$SF_{el} = \frac{\tau_{max}\ L_{per}}{\lambda_{el}} \sin\left\{\arccos\left\{\frac{s_{max} - \Delta_{rebar}}{s_{max}}\right\}\right\} \tag{17}$$

where $\lambda_{el} = \sqrt{\frac{L_{per}\ \tau_{max}}{s_{max}\ E_s\ A_s}}$ and Δ_{rebar} is the slip in the reinforcement at the crack face. Note that this is analogous to equation 14. The slip, Δ_{yield}, associated with the yielding of the reinforcement (Figure 6(b)) is

$$\Delta_{yield} = s_{max}\,(1 - \cos(\lambda_{el} l_{el})) \tag{18}$$

where l_{el} can be determined by substituting $P = P_{yield} = A_s\ f_y$ into equation (15) and setting $l = l_{el}$

where $l_{el} = \frac{\arcsin\left(\frac{A_s\ fy\ \lambda_{el}}{\tau_{max}\ L_{per}}\right)}{\lambda_{el}}$

If the slip in the reinforcement is greater than Δ_{yield} the reinforcement undergoes strain hardening and the force is given by:

$$SF_{sh} = A_s f_y + \frac{\tau_{max}\ L_{per}}{\lambda_{sh}} \sin\left\{\arccos\left\{\frac{s_{max} - (\Delta_{rebar} - \Delta_{yield})}{s_{max}}\right\}\right\} \tag{19}$$

where $\lambda_{sh} = \sqrt{\frac{L_{per}\ \tau_{max}}{s_{max}\ E_{sh}\ A_s}}$.

As the applied load is increased, the bar may fracture before the maximum bond capacity is reached at a slip equal to Δ_{fract}. In this case, the bond stress at the crack face is greater than zero and the slip Δ_{fract} is less than s_{max} (Figure 6(c)). The slip that is required to cause the reinforcement steel to fracture is then:

$$\Delta_{fract} = \Delta_{yield} + s_{max}\left(1 - \cos(\lambda_{sh} l_{fract})\right) \tag{20}$$

where l_{fract} is found by substituting $P = \sigma_{fract} - f_y$ in equation (13) and setting $l = l_{fract}$

$$l_{fract} = \frac{\arcsin\left(\frac{A_s\,(\sigma_{fract} - f_y)\lambda_{sh}}{\tau_{max}\,L_{per}}\right)}{\lambda_{sh}} \tag{21}$$

The complete debonding of the reinforcement is a possibility if the slip reaches s_{max} before the reinforcement force reaches its maximum capacity. In this case, the bond stress at the crack face equals zero as shown in Figure 6(d) where l_{sh} equals $l - l_{el}$. Although Haskett et al.'s approach was based on various assumptions regarding the bond and steel behaviour, the importance of equations (17) and (19) is that they provide a direct relationship between the bridging force in the reinforcement and the slip. The slip can then be associated with crack opening measurements.

4.4 Crack opening in concrete

Crack opening is an important indicator when assessing the level of damage in a concrete structure. Gerstle et al. analysed the crack propagation in concrete beams using the cohesive crack concept (Gerstle et al. 1992). To develop a relationship between the crack opening and other concrete properties, they considered a kinematic approach where the movement of components within a system were analysed by attaching a reference frame to each component. It was determined how the various reference frames moved relative to each other by considering the compatibility of stresses and strains in the system. In the developed dimensionless relationship, Gerstle et al. considered two cases for a reinforced concrete beam (Gerstle et al. 1992); when the crack mouth opening $CMOD$ is less than the critical crack opening C_r and when it exceeds the critical opening. When the $CMOD < C_r$ then

$$CMOD = \frac{2\,A^2\,\beta(1+F)}{(1-A)(1-2\,A\,\beta)}\,C_r \tag{22}$$

where $A = \frac{a}{d}$, a is the crack length, d is the effective beam depth, β is a material-scale parameter for concrete $\beta = \frac{f_t\,d}{E_c C_r}$, f_t is the tensile strength of concrete, E_c is the concrete Young's modulus, and $F = \frac{\sigma_c}{f_t}$ where σ_c is the stress in the top fibre of the concrete beam.

When the $CMOD$ exceeds C_r, then

$$CMOD = \frac{2\,A\beta(1+AF)}{(1-A)}\,C_r \tag{23}$$

It is of note that these equations were developed by ignoring the concrete cover and assuming that the steel was located at the bottom of the reinforced beam. The equations provide a direct closed-form solution that connect the crack opening with geometric and material properties of concrete and are thus of interest in the current work.

4.5 Observations from experimental results

An experimental program to study lightly reinforced concrete beams was carried out in the Cambridge University Engineering Department (Fayyad and Lees 2014, 2017). The investigations were undertaken to explore the cracking process in lightly reinforced concrete beams and to observe the details of the localised fracture process zone development (Fayyad and Lees 2017). The beams were subjected to three-point bending. They had different sizes and reinforcement ratios and the experimental results were analysed using a Digital Image Correlation (DIC) technique. The experimental observations identified features that need to be captured in an analytical model (Fayyad and Lees 2017). It was found that the crack initially propagates in the shape of a single slightly curved band. However, the crack bifurcated when it reached the compression zone, as shown in Figure 7 for a typical lightly reinforced concrete beam. The combination of this bifurcation and cracking led to a failure of the compression zone. Another observation was that a considerable increase in the crack mouth opening occurs during the softening stage. This suggests that before branching the cracking process is more about crack

propagation whereas after branching it is more about crack opening. It is therefore deemed important to consider crack propagation, compression softening and rotation together within an analytical solution to gain a better prediction of the RC beam behaviour. However, crack bifurcation theories are beyond the scope of the current work.

5. Integrated fracture-based model

An integrated fracture-based model (IFBM) is proposed to reflect different local phenomena to provide a more accurate analytical solution for the development of flexural cracks in RC beams from the onset of cracking until failure.

5.1 Model assumptions

The following assumptions were postulated: a single vertical flexural crack crosses the beam perpendicular to the longitudinal reinforcement direction; plane sections remain plane beyond the crack opening tension softening and compression softening areas; cohesive forces develop locally between the crack faces and exhibit a linear softening with crack opening; the concrete tensile strength f_t is a material property independent of size, so there is no size-effect on crack initiation, as distinct from propagation; the concrete in compression is linearly elastic until the peak load, thereafter linear compressive softening is assumed; the steel behaves elastically until reaching the yield stress and then exhibits a linear strain hardening behaviour; the reinforcement slips relative to the concrete and complies with an idealised linear bond-stress slip relationship.

5.2 Formulation of IFBM

The crack models presented in the previous sections were combined into a closed-form solution that included constitutive models, material models and local phenomena in the overall equilibrium of forces. To do this, a rectangular RC beam of width b, depth H (effective depth d) and subjected to an external bending moment M was considered (Figure 8). The formulation of the IFBM model considers three stages of behaviour as follows:

T.M. FAYYAD and J.M. LEES, Integrated fracture-based model formulation for RC crack analysis IN: ASCE Journal of Structural Engineering, *to appear*

5.2.1 First stage

Figure 8(a) presents a simplified view of the beam in the first stage. When the tensile stress at the base of the concrete beam reaches the tensile strength of the concrete, the concrete cracks. With increasing applied moment, the crack propagates and its width and length increase while tensile softening takes place. The elastic force in the steel and the compressive force in the concrete also increase. Using the cross section, crack geometries and parameters shown in Figure 8 leads to:

$$d = a' + s + t \tag{24}$$

where $a' = a - c$ and a is crack length, $c = H - d$, s is the distance from the visible crack tip to the neutral axis and t is the depth of the compression zone. When the steel is located at the extreme fibre ($c = 0$), then $a' = a$. Considering the softening behaviour and according to the cohesive model, the tensile stress at the crack tip equals f_t. From the assumption of plane-sections-remain-plane outside of the cracking area, the relationship between the compressive stress in the top of the section σ_c and the tensile strength of the concrete is:

$$t = \frac{\sigma_c}{f_t}\, s \tag{25}$$

Considering the equilibrium of forces in the *x*-direction at the crack interface leads to

$$SF + 0.5\, b\, a\, f_t \left(2 - \frac{CMOD}{C_r}\right) + 0.5\, b\, s\, f_t - 0.5\, b\, \sigma_c t = 0 \tag{26}$$

where *SF* is the steel force. While the reinforcement remains elastic, the elastic steel force SF can be determined as discussed previously as

$$SF = SF_{el} = n\, \frac{\tau_{max}\, L_{per}}{\lambda_{el}} \sin\left\{\arccos\left\{\frac{s_{max} - \Delta_{rebar}}{s_{max}}\right\}\right\} \tag{27}$$

where n is the number of reinforcing bars, L_{per} is the contact perimeter of the reinforcing bar with the surrounding concrete; $L_{per} = \pi\, d_b$ where d_b is the rebar diameter. τ_{max} and s_{max} are the idealised linear bond-slip parameters determined experimentally, $\lambda_{el} = \sqrt{\frac{\tau_{max}\, L_{per}}{s_{max}\, E_s A_s}}$, $E_s A_s$ is the reinforcement elastic modulus and cross sectional area, and Δ_{rebar} is the slip from one side of the crack. Even though

local effects may also contribute to the crack opening, the crack opening displacement at the level of reinforcement COD_s is nevertheless assumed to be equal to the summation of the slip from each side of the crack where $\Delta_{rebar} = \frac{COD_s}{2}$. If $c = 0$, then $COD_s = CMOD$. If $c > 0$, then $COD_s = CMOD\ \left(\frac{a-c}{a}\right)$. Hence SF_{el} can be determined as a function of $CMOD$ such that

$$SF_{el} = n\ \frac{\tau_{max}\ L_{per}}{\lambda_{el}} \sin\left\{\arccos\left\{\frac{s_{max} - \left(\frac{CMOD\ \left(\frac{a-c}{a}\right)}{2}\right)}{s_{max}}\right\}\right\} \tag{28}$$

To solve these equations, a connection between the $CMOD$ and the stress in the concrete is required. As discussed previously, a formulation for the crack opening displacement at the level of reinforcement COD_s as a function of σ_c has been developed (Gerstle et al. 1992). In Gerstle et al.'s model $a = a'$ because c was assumed to equal zero. However, the $CMOD$ can be calculated such that $CMOD = COD_s\ \left(\frac{a}{a-c}\right)$. Rewriting equation (22) to allow for $c \neq 0$ results in

$$CMOD = \left(\frac{a}{a-c}\right)\left(\frac{2\ (\frac{a'}{d})^2\left(\frac{f_t\ d}{E_c C_r}\right)(1+\frac{\sigma_c}{f_t})}{\left(1-\frac{a'}{d}\right)\left(1-2\ \left(\frac{a'}{d}\right)\left(\frac{f_t\ d}{E_c C_r}\right)\right)}\ C_r\right) \tag{29}$$

In this first stage, for each assumed value of crack length a, the associated values of s, t, σ_c, $CMOD$, and SF can be determined by solving equations 24, 25, 26, 28 and 29. This requires knowledge of the beam geometrical properties (H, d, b, c), concrete properties (f_c, f_t, C_r, E_c) and reinforcement properties (s_{max}, τ_{max}, E_s, E_{sh}, d_b, n, A_s). This first stage describes the behaviour until the tensile stress in the concrete reaches f_t, hence, the $CMOD$ reaches C_r and concrete tensile softening starts. The moment (calculated at the reinforcement level) is then:

$$M = 0.5\ b\ a\ f_t\left(2 - \frac{CMOD}{C_r}\right)\left(\left(\frac{a\left(2\ f_t + f_t\ \left(1 - \frac{CMOD}{C_r}\right)\right)}{3\left(f_t + f_t\ \left(1 - \frac{CMOD}{C_r}\right)\right)}\right) - c\right) \quad (30)$$

$$+\ 0.5\ b\ s\ f_t\ \left(a' + \frac{s}{3}\right) -\ 0.5\ b\ \sigma_c t\left(d - \frac{t}{3}\right)$$

5.2.2 Second stage

The second stage starts when the $CMOD$ exceeds C_r and the concrete at the bottom fibre of the beam cannot sustain any tensile stresses. The stress transfer in the second stage is similar to that of the first stage except for this loss of concrete tensile strength and the subsequent onset of tension softening. So the equilibrium of forces results in;

$$SF +\ 0.5\ b\ a\ f_t\left(\ \frac{C_r}{CMOD}\right) +\ 0.5\ b\ s\ f_t\ -\ 0.5\ b\ \sigma_c t = 0 \quad (31)$$

which is applicable when $CMOD = C_r$ and when $CMOD > C_r$.

There is a possibility for the reinforcement to either remain elastic or to yield, so both cases are considered. When the steel is elastic $SF = SF_{el}$ equation (28) applies. But when the steel yields ($SF = SF_{sh}$) and

$$SF_{sh} = n\ \frac{\tau_{max}\ L_{per}}{\lambda_{sh}} \sin\left\{\arccos\left\{1 - \frac{\left(\left(\frac{CMOD\ \left(\frac{a-c}{a}\right)}{2}\right) - \Delta_{yield}\right)}{s_{max}}\right\}\right\} +\ A_s f_y \quad (32)$$

where $\lambda_{sh} = \sqrt{\frac{L_{per}\ \tau_{max}}{s_{max}\ E_{sh}\ A_s}}$

The reinforcement yields if $\Delta_{rebar} \geq \Delta_{yield}$, where $\Delta_{rebar} = \frac{COD_s}{2}$ and $\Delta_{yield} = s_{max}\,(1 - \cos(\lambda_{el} a_{el}))$ and $a_{el} = \frac{\arcsin\left(\frac{A_s\ f_y\ \lambda_{el}}{\tau_{max}\ L_{per}}\right)}{\lambda_{el}}$. The value of Δ_{fract} should be calculated to determine when

steel ruptures such that $\Delta_{fract} = \Delta_{yield} + s_{max}\left(1 - \cos(\lambda_{sh} a_{fract})\right)$ where $a_{fract} = \frac{\arcsin\left(\frac{A_s(\sigma_{fract} - f_y)\lambda_{el}}{\tau_{max} L_{per}}\right)}{\lambda_{sh}}$.

The reinforcement yield strength f_y and fracture strength σ_{fract} are required for the solution of the stage II crack development.

When $CMOD > C_r$ and $c \neq 0$, the relationship between $CMOD$ and σ_c based on (Gerstle et al. 1992) is:

$$CMOD = \left(\frac{a}{a-c}\right)\left(\frac{2\left(\frac{a'}{d}\right)\left(\frac{f_t\, d}{E_c C_r}\right)\left(1 + \left(\frac{a'}{d}\right)\left(\frac{\sigma_c}{f_t}\right)\right)}{\left(1 - \frac{a'}{d}\right)} C_r\right) \tag{33}$$

Similar to the first stage, the cracking parameters can be determined by solving equations 24, 25, 31 and either 28 and 29 or 32 and 33. At each step, the values of SF and COD_s should be compared with the values of $\sigma_{fract}\, A_s$ and s_{max} respectively. The beam fails due to reinforcement fracture if SF reaches $\sigma_{fract}\, A_s$ or due to reinforcement slippage if the COD_s exceeds twice the value of s_{max}. The moment (calculated at the reinforcement level) is:

$$M = 0.5\, b\, f_t\, a\left(\frac{C_r}{CMOD}\right)\left(a' - \left(\frac{1}{3}\left(a\,\frac{C_r}{CMOD}\right)\right)\right) + 0.5\, b\, s\, f_t\left(a' + \frac{s}{3}\right) - 0.5\, b\, \sigma_c t\left(d - \frac{t}{3}\right) \tag{34}$$

5.2.3 Third stage

If the beam has not previously failed due to reinforcement rupture or reinforcement slippage, the third stage predicts the RC beam behaviour when the concrete in compression exhibits softening. It is assumed that the softening starts from the top fibre of the beam where the maximum concrete compressive stress exists. If the depth of the compressive softening is denoted as x then

$$d = a' + s + t' + x \tag{35}$$

and

$$t' = \frac{f_c}{f_t}\, s \tag{36}$$

The introduction of x as a new variable requires the establishment of a new relationship between x and the material properties in order to develop a closed-form solution.

According to Figure 8(d):

$$x = t' \left(\frac{\varepsilon_c - \varepsilon_0}{\varepsilon_0}\right) \tag{37}$$

where ε_0 is the strain corresponding to the compressive strength f_c. With an assumption of linear softening, the compression strain at the top of the beam can be calculated from equation (3) and the required parameters can be considered to be material properties of concrete (Borges et al. 2004). Substituting the value of ε_c from equation (3) into equation (37) leads to:

$$x = t' \left(\frac{\varepsilon_{cr}\left(1 - \frac{\sigma_c}{f_c}\right) + \varepsilon_0\left(\frac{\sigma_c}{f_c}\right) - \varepsilon_0}{\varepsilon_0}\right) \tag{38}$$

Longitudinal force equilibrium gives

$$SF + 0.5\, b\, a\, f_t\left(\frac{C_r}{CMOD}\right) + 0.5\, b\, s\, f_t - 0.5\, b\, f_c t' - 0.5\, b\, x\, (\sigma_c + f_c) = 0 \tag{39}$$

The relationship between $CMOD$ and σ_c presented for the second stage (equation (33)) can be modified to find a relationship between $CMOD$ and x as follows:

$$CMOD = \left(\frac{a}{a-c}\right)\left(\frac{2\left(\frac{a'}{d-x}\right)\left(\frac{f_t(d-x)}{E_c C_r}\right)\left(1 + \left(\frac{a'}{d-x}\right)\left(\frac{f_c}{f_t}\right)\right)}{\left(1 - \frac{a'}{d-x}\right)}\, C_r\right) \tag{40}$$

and SF can be determined using equation (28) or (32) as appropriate.

The moment (calculated at the reinforcement level) is:

$$M = 0.5\, b\ f_t\, a \left(\frac{C_r}{CMOD}\right)\left(a' - \left(\frac{1}{3}\left(a\ \frac{C_r}{CMOD}\right)\right)\right) + 0.5\, b\, s\, f_t \left(a' + \frac{s}{3}\right) - 0.5\, b\, f_c\, t' \left(a' + \frac{2\, t'}{3}\right) - 0.5\, b\, x\, (\sigma_c + f_c)\left(d - \left(\frac{x\,(2f_c + \sigma_c)}{3(f_c + \sigma_c)}\right)\right) \quad (41)$$

It is of note that the crack tip during this stage is close to the neutral axis and once the crack reaches the compression zone, there is crack opening and rotation around the crack tip. The beam might fail due to reinforcement fracture, reinforcement slippage or concrete crushing; whichever occurs first.

5.2.4 Solution procedure for mode I cracking

Considering the three stages indicated in the previous sections, the crack propagation of lightly reinforced concrete beams can be modelled by solving the associated equations for given material and geometrical properties. In the current paper, the equations were solved using Matlab software. The IFBM formulation has been derived for a single crack. In lightly reinforced concrete beams a single flexural crack can initiate and dominate the failure process and hence a single crack analysis provides detailed insight. The extension of the model to beams that exhibit multiple cracks could be based on a framework where each crack is considered in turn e.g. as has been applied in rigid block analyses (Lees and Burgoyne 2000), or partial interaction theory (Oehlers et al. 2005). However, further investigations would be required to take into account multiple cracks.

5.3 Discussion of the proposed model

5.3.1 Model outcome

Using the proposed model, a full description of the cracking process can be developed for different material properties and beams of different sizes. Figure 9 shows the predicted dimensionless moment $\left(\frac{M}{f_c b\, d^2}\right)$ versus relative crack length $\left(\frac{a}{d}\right)$ for an RC beam with the properties shown in Table 1 and for different reinforcement ratios (0.14% - 2%). There are some kinks in the graphs which indicate a change between the different stages of behaviour. With sufficient reinforcement, the crack propagates with increasing applied moment. However, with low reinforcement ratios, in some regions, the applied moment shows a decrease in capacity with crack propagation.

T.M. FAYYAD and J.M. LEES, Integrated fracture-based model formulation for RC crack analysis IN: ASCE Journal of Structural Engineering, *to appear*

The model assumes a gradual loss of tensile strength with crack propagation and that the concrete loses its tensile strength completely when the crack mouth opening equals the critical crack opening C_r. For the modelled beams, the point at which there is a decrease in the moment capacity is associated with the complete loss of the tensile stresses at the crack mouth as shown in Figure 9. These stresses are then transferred to the reinforcement. If the initial increase in the reinforcement force is not sufficient to compensate for the loss of the concrete tensile stresses, the resistance decreases causing unstable crack propagation as noted for the beams with reinforcement ratios between 0.14 and 0.77%. When $\rho > 0.8\%$, the resisting moment remains greater than the moment at the onset of unstable crack growth. Stable behaviour is associated with the development of the crack with increasing load whereas unstable behaviour is associated with the propagation of the crack under decreasing load. Reinforcement fracture occurs when the predicted reinforcement strain reaches the steel fracture strain. With higher reinforcement ratios, the crack propagation stage includes tensile softening until the tensile stresses diminish. If the stresses in the concrete reach the compressive strength, f_c, the concrete in compression softens before failure and this depends on the geometrical and material properties. However, once the critical compressive damage strain is reached, the concrete fails due to concrete crushing. The crack length at failure depends on the geometrical and material properties as these dictate the occurrence and sequence of possible outcomes e.g. fracture, debonding, and crushing.

The cracking process cannot be fully explained by the relative crack length development in isolation. The crack mouth opening is another important parameter that the model can predict. Figure 10 shows the $CMOD$ results for selected beams. For each of the selected beams, the point at which the crack length reaches seventy percent of its final crack length (L70) is indicated in the figure. Even when the crack length has reached 70%, it can be seen that the crack opening is only a relatively small fraction of the final $CMOD$. The proposed model predictions therefore demonstrate a crack propagation phase followed by a crack rotation phase and these stages depend on the properties of the concrete and the reinforcement. The $CMOD$ values increase with increasing reinforcement ratios. In the beams with reinforcement ratios of 0.14% and 0.4%, the opening of the crack is associated with a relatively constant value of dimensionless moment. So any increase in the applied moment above the beam capacity will

lead to sudden failure and the horizontal path will not necessarily be observed. By increasing the reinforcement ratio to 0.77%, around 93% of the crack opening occurs after a crack length that is 70% of the final length. Also, the crack opening is associated with an increase in the beam capacity and this gives more ductile behaviour when compared with beams with lower reinforcement ratios (Fayyad and Lees 2015). However, this increase in the ductility was not sufficient to ensure a final ductile failure and the beam failed due to a sudden reinforcement fracture. The model is therefore capable of predicting the different stages of cracking.

The results in Figures 9 and 10 are for beams with the specific material and geometric properties noted in Table 1. The predicted zones of unstable crack growth and failure sequences depend on the input parameters. Even for a given reinforcement ratio, different outcomes would be expected for beams with different sizes, concrete properties etc. So the results shown in the figures cannot be generalised. However, the fundamental nature of the IFBM allows for an exploration of these inter-dependencies to extract features such the reinforcement ratio where the failure would be predicted to change from reinforcement fracture to concrete crushing.

5.3.2 Analytical and experimental results

The model was further verified by comparing analytical predictions with experimental data presented in Fayyad and Lees (2017). The beams had different sizes (beam heights of 120 mm, 220 mm or 320 mm) and different reinforcement ratios (0.15%, 0.2%, 0.3%, 0.4% or 0.5%) as summarised in Table 2. The material properties shown in Table 3 were obtained by testing control samples with the exception of ε_{cr} and C_r which were calculated using the equations indicated. Any inaccuracies in the measured experimental input parameters will influence the quality of the predictions. The experimental crack lengths were measured using a DIC technique and were calculated as the vertical distance to the crack tip from the base of the beam.

All the beams appeared to fail due to reinforcement fracture. Figures 11, 12 and 13 show a comparison between the applied load versus crack length analytical predictions and experimental results for the three beam sizes. For the medium sized beams M30,H220,0.15,FD and M30,H220,0.3,FD with a

concrete strength of 30MPa (see Figure 12), the theoretical predictions are a good match with the experimental results and these two beams failed due to reinforcement fracture as predicted by the IFBM. The crack propagated quickly in beam M30,H220,0.15,FD in the unstable crack propagation region and this made it difficult to measure the crack length between 120 mm and 170 mm. In beam M30,H220,0.4,FD, at the beginning of the crack propagation stage the experimental measurements of crack length were slightly lower than those predicted by the models. With the development of the crack, the differences between the predicted values and the measured values increased with the applied load. This was thought to be because in beam M30,H220,0.4,FD several flexural cracks formed in the beam span as shown in Figure 14 whereas the proposed model only modelled a single flexural crack. Although the crack length measurements were lower than the predicted values, the overall behavioural trends were consistent with the predictions.

The experimental results versus theoretical predictions for the beams with heights of 320 mm and 120 mm are shown in Figures 13 and 11 respectively. In beams M45,H320,0.2,FD and M45,H320,0.3,FD (Figure 13) and beams M45,H120,0.3,FD and M45,H120,0.5,FD (Figure 11) there is a good match between the experimental results and the theoretical predictions but the descending "unstable cracking branches" are not always captured. It is believed that this was due to the beams being tested under displacement control. To get a better indication of a decreasing branch in the crack length-moment diagram, the beams should be tested under *CMOD* controlled tests. It was not possible to take measurements of the crack length in beam M45,H320,0.3,FD near failure because of a problem with the main camera (see (Fayyad and Lees 2017) for further details). Hence, the peak load is marked on the figure but the equivalent crack length is unknown.

5.3.3 Comparisons with other models

In order to benchmark the IFBM model, the IBFM and experimental results for a typical reinforced beam (M30,H220,0.15,FD) were compared with predictions from selected theoretical models in the literature as shown in Figure 15. The bridged crack model proposed by Carpinteri (1984) is one of the earliest models that applied fracture mechanics to the tensile cracking of RC structures and has acted as the basis for subsequent models. In the original model, Carpinteri used the concept of superposition to

add the stress intensity contributions from the applied load and the reinforcement. The bridged crack model is based on LEFM so the fracture process zone ahead of the crack tip is ignored. Unlike the IFBM, it also assumes that any bond effects do not influence the concrete crack propagation and the force distribution in the compression zone is not considered in detail. As such, according to the model, the dimensionless bending moment associated with the crack propagation only depends on the relative crack depth for a given brittleness number. Gerstle et al's model (Gerstle et al. 1992) is an NLFM model that considers the softening that occurs in the tension zone with some assumptions about the cohesive model. A dimensionless moment was obtained as a function of the crack length for given concrete and steel properties. The IFBM similarly considers the tension softening using a force balance and both of the models are able to predict the crack initiation. However, Gerstle et al's model does not consider the bond-slip behaviour nor the softening of concrete in compression or strain hardening of the reinforcement after yielding. Hence, in the later stages of the loading, the IFBM describes the post-yielding behaviour in more detail since it considers these contributions. Gerstle et al's model predicts unstable crack propagation in beam M30,H220,0.15,FD under decreasing load. However, if the load during testing was maintained there would be a jump in the solution (represented with the region denoted by arrows in Figure 15) that would lead to a fairly good prediction of the relative crack length versus load. Haskett et al. (2009a) introduced a rigid body moment-rotation mechanism for RC beam hinges. Shear-friction theory was used to quantify the softening force in the compression zone. The rotation that occurs around the crack tip takes into account compression softening and concrete-reinforcement interaction. Although the model is able to predict the behaviour when the beam is fully cracked, it is not able to describe the crack propagation since it concentrates on the crack rotation stage after the crack has developed and the crack length is fairly constant.

In summary, the bridged crack model and Gerstle et al's model mainly consider the crack propagation stage, whereas Haskett et al's model considers crack rotation. It can be seen in Figure 15 that the actual beam behaviour exhibits features that are partly consistent with Gerstle et al.'s model and partly with Haskett et al.'s. This highlights the importance of combining the tension cohesive stress, bond-slip behaviour and compression softening when studying the cracking mechanism of RC beams. The IFBM

predicts the crack propagation stage taking into account the reinforcement-concrete interaction and this leads to more accurate crack length versus load predictions. The inclusion of compressive softening in the equilibrium and compatibility equations, albeit in a simplified manner, also led to a more realistic prediction of the cracking behaviour until beam failure.

6. Conclusions

To bridge the gap between a 'structural view' and a 'fracture view' of the cracking process in lightly reinforced concrete, an integrated fracture-based model (IFBM) was developed to predict the behaviour of lightly reinforced concrete beams. The proposed model is a closed-form solution that incorporates post-cracking tensile stresses in the concrete, the bond-slip behaviour between the reinforcement and concrete, and compression softening in the concrete compressive zone. The IFBM was formulated in terms of equilibrium, compatibility and constitutive considerations. The stages of the analysis included the development of a crack, crack propagation with tension softening, concrete compressive softening and rotation. It was found that the incorporation of local phenomena into a global equilibrium formulation enabled the development of a more rational crack behaviour model. The model was capable of describing the cracking process in reinforced concrete including the initiation and propagation of a flexural crack. It was also able to describe the post-yielding behaviour since it considers the softening of concrete in compression and the strain hardening of the reinforcement after yielding. The model predictions show a fairly good agreement with experimental observations of the cracking process of a single flexural crack in lightly reinforced concrete beams. The IFBM formulation has a tractable solution procedure that captures the influences of core material and geometric properties on the mode I fracture behaviour. This provides a rational basis for a detailed analysis of cracks in concrete, and to inform minimum reinforcement requirements.

Acknowledgements

The authors would like to thank the Yousef Jameel Foundation and Cambridge Overseas Trust (COT) for their financial support of this research.

References

Bazant, Z. P., and Kazemi, M. T. (1990). "Determination of fracture energy, process zone length and

T.M. FAYYAD and J.M. LEES, Integrated fracture-based model formulation for RC crack analysis IN: ASCE Journal of Structural Engineering, *to appear*

brittleness number from size effect, with application to rock and conerete." *International Journal of Fracture*, 44(2), 111–131.

Bazant, Z. P., and Kim, J. K. (1984). "Size effect in shear failure of longitudinally reinforced beams." *ACI Journal*, 81(38), 456–468.

Bažant, Z. P., and Oh, B. H. (1983). "Crack band theory for fracture of concrete." *Matériaux et Constructions*, 16(3), 155–177.

Bažant, Z. P., Pan, J., and Pijaudier-Cabot, G. (1987). "Softening in reinforced concrete beams and frames." *Journal of Structural Engineering*, American Society of Civil Engineers, 113(12), 2333–2347.

Bigaj, A., and Walraven, J. (2002). "Size effects in plastic hinges of reinforced concrete members." *Heron*, 47(1), 79–80.

Borges, J. U. A., Subramaniam, K. V., Weiss, W. J., Shah, S. P., and Bittencourt, T. N. (2004). "Length effect on ductility of concrete in uniaxial and flexural compression." *ACI Structural Journal*, 101(6), 765–772.

Bosco, C., and Carpinteri, A. (1992). "Fracture behavior of beam cracked across reinforcement." *Theoretical and Applied Fracture Mechanics*, 17(1), 61–68.

Carpinteri, A. (1984). "Stability of fracturing process in RC beams." *Journal of Structural Engineering*, 110(3), 544–558.

Carpinteri, A., Carmona, J. R., and Ventura, G. (2007). "Propagation of flexural and shear cracks through reinforced concrete beams by the bridged crack model." *Magazine of Concrete Research*, Thomas Telford, 59(10), 743–756.

Carpinteri, A., Corrado, M., Paggi, M., and Mancini, G. (2009). "New model for the analysis of size-scale effects on the ductility of reinforced concrete elements in bending." *Journal of Engineering Mechanics*, 135(March), 221–229.

Carpinteri, A., and Massabo, R. (1997). "Continuous vs discontinuous bridged-crack model for fiber-reinforced materials in flexure." *International Journal of Solids and Structures*, 34(18), 2321–2338.

Casanova, A., Jason, L., and Davenne, L. (2012). "Bond slip model for the simulation of reinforced concrete structures." *Engineering Structures*, 39, 66–78.

Cedolin, L., Dei Poli, S., and Iori, I. (1983). "Experimental determination of the fracture process zone in concrete." *Cement and Concrete Research*, 13(4), 557–567.

Chan, B. H. C., Cheung, Y. K., and Huang, Y. P. (1993). "Crack analysis of reinforced concrete tension members." *Journal of Structural Engineering*, 118, 2118–2132.

Chen, H. H., and Su, R. K. L. (2013). "Tension softening curves of plain concrete." *Construction and Building Materials*, 44, 440–451.

Crisfield, M. A. (1982). "Local instabilities in the non-linear analysis of reinforced concrete beams and slabs." *Proc. Instn Civ. Engrs, Part 2*, 73(Mar), 135–145.

Deng, P., and Matsumoto, T. (2017). "Estimation of the rebar force in RC members from the analysis of the crack mouth opening displacement based on fracture mechanics." *Journal of Advanced Concrete Technology*, Japan Concrete Institute, 15(2), 81–93.

Eligehausen, R., Popov, E. P., and Bertero, V. V. (1982). "Local bond stress-slip relationships of deformed bars under generalized excitations." *Earthquake Engineering Research Center Report*, University of California, Berkeley.

Elmorsi, M. (2000). "Modeling bond-slip deformations in reinforced concrete beam-column joints." *Canadian Journal of Civil Engineering*, 27, 490–505.

Fayyad, T. M., and Lees, J. M. (2014). "Application of digital image correlation to reinforced

concrete fracture." *Procedia Materials Science*, 3, 1585–1590.

Fayyad, T. M., and Lees, J. M. (2015). "Evaluation of a minimum flexural reinforcement ratio using fracture-based modelling." *IABSE 2015– Structural Engineering: Providing Solutions to Global Challenges, Geneva*, Geneva.

Fayyad, T. M., and Lees, J. M. (2017). "Experimental investigation of crack propagation and crack branching in lightly reinforced concrete beams using Digital Image Correlation." *Engineering Fracture Mechanics*, 182, 487–505.

Focacci, F., Nanni, A., and Bakis, C. (2000). "Local bond-slip relationship for FRP reinforcement in concrete." *Journal of Composites for Construction*, 4(1), 24–31.

Gastebled, O., and May, I. (2001). "Fracture mechanics model applied to shear failure of reinforced concrete beams without stirrups." *ACI Structural Journal*, 98(2), 184–190.

Gerstle, W. H., Dey, P. P., Prasad, N. N. V, Rahulkumar, P., and Xie, M. (1992). "Crack growth in flexural members. A fracture mechanics approach." *ACI Structural Journal*, 89(6), 617–625.

Gerstle, W. H., and Xie, M. (1992). "FEM Modeling of Fictitious Crack Propagation in Concrete." *Journal of Engineering Mechanics*, American Society of Civil Engineers, 118(2), 416–434.

Gopalaratnam, V. S., and Shah, S. P. (1985). "Softening response of plain concrete in direct tension." *ACI Journal Proceedings*, 82(3), 310–323.

Griffith, A. (1921). "The phenomena of rupture and flow in solids." *Philosophical Transactions of the Royal Society of London. Series A, Containing Papers of a Mathematical or Physical Character*.

Gustafsson, P. J., and Hillerborg, A. (1988). "Sensitivity in shear strength of longitudinally reinforced concrete beams to fracture energy of concrete." *Structural Journal*, 85(3), 286–294.

Haskett, M., Oehlers, D. J., and Mohamed Ali, M. S. (2008). "Local and global bond characteristics of steel reinforcing bars." *Engineering Structures*, 30(2), 376–383.

Haskett, M., Oehlers, D. J., Mohamed Ali, M. S., and Wu, C. (2009a). "Rigid body moment-rotation mechanism for reinforced concrete beam hinges." *Engineering Structures*, Elsevier Ltd, 31(5), 1032–1041.

Haskett, M., Oehlers, D. J., Mohamed Ali, M. S., and Wu, C. (2009b). "Yield Penetration Hinge Rotation in Reinforced Concrete Beams." *Journal of Structural Engineering*, 135(February), 130–138.

Hillerborg, A. (1990). "Fracture mechanics concepts applied to moment capacity and rotational capacity of reinforced concrete beams." *Engineering Fracture Mechanics*, 35(l), 233–240.

Hillerborg, A., Modéer, M., and Petersson, P. E. (1976). "Analysis of crack formation and crack growth in concrete by means of fracture mechanics and finite elements." *Cement and Concrete Research*, 6(6), 773–781.

Hognestad, E., Hanson, N. W., and McHenry, D. (1955). "Concrete stress distribution in ultimate strength design." *ACI Journal Proceedings*, 52(12), 455–480.

Ingraffea, A. R., Gerstk, W. H., Gergely, P., and Saouma, V. (1984). "Fracture mechanics of bond in reinforced concrete." *Journal of Structural Engineering*, American Society of Civil Engineers, 110(4), 871–890.

Jansen, D. C., and Shah, S. P. (1997). "Effect of length on compressive strain softening of concrete." *Journal of Engineering Mechanics*, 123, 25–35.

Jenq, Y. S., and Shah, S. P. (1988). "Mixed-mode fracture of concrete." *International Journal of Fracture*, Kluwer Academic Publishers, 38(2), 123–142.

Jenq, Y. S., and Shah, S. P. (1990). "Shear resistance of reinforced concrete beams- A fracture mechanics approach." *ACI Special Publication*, 118, 237–258.

Jenq, Y., and Shah, S. P. (1985). "Two parameter fracture model for concrete." *Journal of Engineering Mechanics*, American Society of Civil Engineers, 111(10), 1227–1241.

Kaplan, M. F. (1961). "Crack propagation and the fracture of concrete." *ACI Journal Proceedings*, 58(11), 591–610.

Karihaloo, B. L., and Nallathambi, P. (1989). "An improved effective crack model for the determination of fracture toughness of concrete." *Cement and Concrete Research*, 19(4), 603–610.

Kheyroddin, A., and Naderpour, H. (2007). "Plastic hinge rotation capacity of reinforced concrete beams." *Int. J. Civ. Eng*, 5(1), 30–47.

Lees, J. M., and Burgoyne, C. J. (1999). "Transfer bond stresses generated between FRP tendons and concrete." *Magazine of Concrete Research*, 51(4), 229–239.

Lees, J. M., and Burgoyne, C. J. (2000). "Analysis of concrete beams with partially bonded composite reinforcement." *ACI Structural Journal*, 97(2), 252–258.

Li, V. C., Chan, C.-M., and Leung, C. K. Y. (1987). "Experimental determination of the tension-softening relations for cementitious composites." *Cement and Concrete Research*, 17(3), 441–452.

Lopes, S., and Bernardo, L. (2003). "Plastic rotation capacity of high-strength concrete beams." *Materials and Structures*, 36, 22–31.

Luchko, I. I. (1996). "Basic concepts of the fracture mechanics of reinforced concrete." *Materials Science*, 31(4), 448–453.

Manfredi, G. (1998). "Evaluation of the rotation capacity in RC beams including size effect." *CEB Bulletin d'Information No.242- Ductility of Reinforced Concrete Structures - The International Federation for Structural Concrete*.

Markeset, G., and Hillerborg, A. (1995). "Softening of concrete in compression — Localization and size effects." *Cement and Concrete Research*, 25(4), 702–708.

Martin, H. (1973). "On the interrelation among surface roughness, bond and bar stiffness in the reinforcement subject to short-term loading." *Deutscher Ausschuss Stahlbeton*, 228, 1–50.

Mi, Z., Li, Q., Hu, Y., Xu, Q., and Shi, J. (2016). "An analytical solution for evaluating the effect of steel bars in cracked concrete." *Engineering Fracture Mechanics*, 163, 381–395.

van Mier, J. G. M. (1995). "Fracture mechanics of concrete: Will applications start to emerge?" *HERON, 40 (2), 1995*, Delft University of Technology.

van Mier, J. (1984). "Strain-softening of concrete under multiaxial loading conditions." PhD thesis, Technical University of Eidhoven.

Mirza, S. M., and Houde, J. (1979). "Study of bond stress-slip relationships in reinforced concrete." *ACI Journal*, 76(1), 19–46.

Mohamed Ali, M. S., Oehlers, D. J., Griffith, M. C., and Seracino, R. (2008). "Interfacial stress transfer of near surface-mounted FRP-to-concrete joints." *Engineering Structures*, 30(7), 1861–1868.

Nemati, K., Monteiro, P., and Scrivener, K. (1998). "Analysis of compressive stress-induced cracks in concrete." *ACI Materials Journal*, 95(5), 617–630.

Nomura, N., Mihashi, H., and Izumi, M. (1991). "Correlation of fracture process zone and tension softening behavior in concrete." *Cement and Concrete Research*, 21(4), 545–550.

Oehlers, D. J., Liu, I. S. T., and Seracino, R. (2005). "The gradual formation of hinges throughout reinforced concrete beams." *Mechanics Based Design of Structures and Machines*, Taylor & Francis Group, 33(3–4), 373–398.

Oehlers, D. J., Visintin, P., Chen, J.-F., Seracino, R., Wu, Y., and Lucas, W. (2017). "Reinforced concrete behavior, research, development, and design through partial-interaction mechanics." *Journal of Structural Engineering*, 143(7), 2517002.

Ohno, K., Uji, K., Ueno, A., and Ohtsu, M. (2014). "Fracture process zone in notched concrete beam under three-point bending by acoustic emission." *Construction and Building Materials*, Elsevier Ltd, 67, 139–145.

Ooi, E. T., and Yang, Z. J. (2011). "Modelling crack propagation in reinforced concrete using a hybrid finite element-scaled boundary finite element method." *Engineering Fracture Mechanics*, Elsevier Ltd, 78(2), 252–273.

Paggi, M., Corrado, M., Mancini, G., and Carpinteri, A. (2009). "The overlapping crack model for uniaxial and eccentric concrete compression tests." *Magazine of Concrete Research*, 61(9), 745–757.

Rehm, G. (1961). "On the fundamentals of steel-concrete bond." *Deutscher Ausschuss für Stahlbeton*, 138, 1–59.

Saleh, A. L., and Aliabadi, M. H. (1998). "Crack growth analysis in reinforced concrete using BEM." *Journal of Engineering Mechanics*, American Society of Civil Engineers, 124(9), 949–958.

Seracino, R., Raizal Saifulnaz, M. R., and Oehlers, D. J. (2007). "Generic debonding resistance of EB and NSM plate-to-concrete joints." *Journal of Composites for Construction*, American Society of Civil Engineers, 11(1), 62–70.

Shah, S., and Sankar, R. (1987). "Internal cracking and strain softening response of concrete under uniaxial compression." *ACI Materials Journal*, 84(3), 200–212.

So, K. O., and Karihaloo, B. L. (1993). "Shear capacity of longitudinally reinforced beams-A fracture mechanics approach." *Structural Journal*, 90(6), 591–600.

Thorenfeldt, E., Tomaszewicz, A., and Jensen, J. (1987). "Mechanical properties of high-strength concrete and application in design." *Proceedings of the symposium utilization of high strength concrete*, Norway: Tapir Trondheim, 149–159.

Torrenti, J. M., Benaija, E. H., and Boulay, C. (1993). "Influence of boundary conditions on strain softening in concrete compression test." *J. Eng. Mech.*, 119, 2369–2384.

van Vliet, M., and van Mier, J. (1996). "Experimental investigation of concrete fracture under uniaxial compression." *Mechanics of Cohesive-frictional materials*, 1, 115–127.

Walraven, J. (2007). "Fracture mechanics of concrete and its role in explaining structural behaviour." *6th International Conference on Fracture Mechanics of Concrete and Concrete Structures, Catania, Italy*, Catania, Italy.

Watanabe, K., Niwa, J., Iwanami, M., and Yokota, H. (2004). "Localized failure of concrete in compression identified by AE method." *Construction and Building Materials*, 18, 189–196.

Wu, Y., and Zhao, X. (2012). "Unified bond stress–slip model for reinforced concrete." *Journal of Structural Engineering*, 139(11), 1951–1962.

Wu, Z., Yuan, H., and Niu, H. (2002). "Stress Transfer and Fracture Propagation in Different Kinds of Adhesive Joints." *Journal of Engineering Mechanics*, American Society of Civil Engineers, 128(5), 562–573.

Yuan, H., Teng, J. G., Seracino, R., Wu, Z. S., and Yao, J. (2004). "Full-range behavior of FRP-to-concrete bonded joints." *Engineering Structures*, 26, 553–565.

Nomenclature

a	Crack length
a'	Crack length excluding the concrete cover
A	Dimensionless parameter
A_c	Cross sectional area of concrete element
A_s	Cross sectional area of steel bar
b	Beam width
c	Concrete cover
C_r	Critical crack width in concrete beam
CF	Total closing force due to concrete tensile softening
COD_s	Crack opening displacement at the level of reinforcement
d	Effective beam depth
d_b	Bar diameter
E_c	Young's modulus of elasticity of concrete
E_s	Young's modulus of elasticity of steel reinforcement
E_{sh}	Strain hardening modulus
f_c	Average concrete compressive cube strength
f_t	Direct tensile strength of concrete
f_y	Reinforcement yielding strength
H	Total beam depth
K	Stress intensity factor of a material
L	Pull-out specimen length

L_{per}	Contact perimeter of the reinforcement at the interface with the surrounding concrete
l	Length of reinforcement bar where slip has developed
l_{cr}	A critical length where the bond-slip is fully developed
l_{el}	Length of the reinforcement bar where slip has developed at the point when the reinforcement yields
l_{fract}	Length of the reinforcement bar where slip has developed at the point when the reinforcement fractures
l_{sh}	Post-yield length of the reinforcement bar where slip has developed (equal to $l - l_{el}$)
M	Bending moment
n	Number of reinforcing bars in a beam
P	Reinforcement force in a pull-out test
P_d	Debonding reinforcement force
P_{max}	Maximum reinforcement force in a pull-out test
SF	Steel force
SF_{el}	Elastic steel force
SF_{sh}	Strain hardening steel force
s	Bond slip, or distance from the visible crack tip to the neutral axis
s_{max}	Maximum bond slip
t'	Depth of the compression zone excluding depth of the compressive softening
w	Crack width
w_c	Critical crack width
x	Depth of the compressive softening, or distance along pull-out specimen
β	Material scale parameter
Δ_{fract}	Slip in the reinforcement bar that is required to cause fracture
Δ_{rebar}	Slip in the reinforcement at the crack face
Δ_{yield}	Slip that is required to cause the reinforcement bar to yield
ε_c	Strain in the concrete
ε_{cr}	Critical damage strain
ε_{fract}	Strain at fracture
ε_0	Strain corresponding to the peak compressive strength

ε_s	Strain in the reinforcement
ε_y	Yielding strain in the reinforcement
λ	Constant that reflects reinforcement-concrete interaction properties
λ_{el}	Constant that reflects reinforcement-concrete interaction properties in the elastic stage
λ_{sh}	Constant that reflects reinforcement-concrete interaction properties after reinforcement yielding
σ	Stress
σ_c	Stress in the concrete
σ_{fract}	Stress at reinforcement fracture
σ_s	Stress in the reinforcement
τ	Bond stress
τ_{max}	Maximum bond strength

Abbreviations

BCM	Bridged crack model
CCM	Cohesive crack model
CMOD	Crack mouth opening displacement
DIC	Digital image correlation
FCM	Fictitious crack model
FRP	Fibre reinforced polymers
FRZ	Fracture process zone
IFBM	Integrated fracture-based model
LEFM	Linear elastic fracture mechanics
NLFM	Non-linear fracture mechanics
RC	Reinforced concrete

Table 1: Material properties of the modelled RC beams

Beam width (b)	100 mm
Beam depth (d)	200 mm
Beam cover (c)	20 mm
Concrete compressive strength (f_c)	45 MPa
Concrete tensile strength (f_t)	5.6 MPa
Elastic modulus of concrete (E_c)	36400 MPa
Critical *CMOD* (C_r)	0.07 mm
Steel yielding stress (f_y)	540 MPa
Maximum shear strength (τ_{max})	9 MPa
Elastic modulus of steel (E_s)	205000 MPa
Strain corresponding to f_c (ε_0)	0.002
Critical damage strain (ε_{cr})	0.0075*

* calculated as $\varepsilon_{cr} = 0.0129\, e^{(-0.012\, f_c)}$ (Borges et al. 2004)

Table 2: Properties of test beams (Fayyad and Lees 2017)

Concrete compressive strength (MPa)	**Beam dimensions H×W×L (mm×mm × mm)**	**Reinforcement (ratio)**	**Notation**
30	220×100×1700	1T6 (0.15%)	M30,H220,0.15,FD
		2T6 (0.3%)	M30,H220,0.3,FD
		3T6 (0.4%)	M30,H220,0.4,FD
45	320×100×2500	2T6 (0.2%)	M45,H320,0.2,FD
		3T6 (0.3%)	M45,H320,0.3,FD
	120×100×840	1T6 (0.3%)	M45,H120,0.3,FD
		1T8 (0.5%)	M45,H120,0.5,FD

Table 3: Parameters used in experimental predictions (Fayyad and Lees 2017)

Concrete compressive strength (f_c)	45 MPa	30MPa
Concrete tensile strength (f_t)	5.6 MPa	4MPa
Elastic modulus of concrete (E_c)	36400MPa	27500MPa
Critical damage strain (ε_{cr})	0.0075*	0.009*
Critical CMOD (C_r)	0.07** mm	0.08**
Fracture toughness (G_{IC})	107N/m	93N/m
Steel yield stress (f_y)	540 MPa	
Maximum shear strength (τ_{max})	9 MPa	
Elastic modulus of steel (E_s)	205000 MPa	

* calculated as $\varepsilon_{cr} = 0.0129\, e^{(-0.012\, f_c)}$ (Borges et al. 2004)

** calculated as $C_r = \frac{3.6 G_{IC}}{f_t}$ (Gustafsson and Hillerborg 1988); G_{IC} is the fracture toughness of the material.

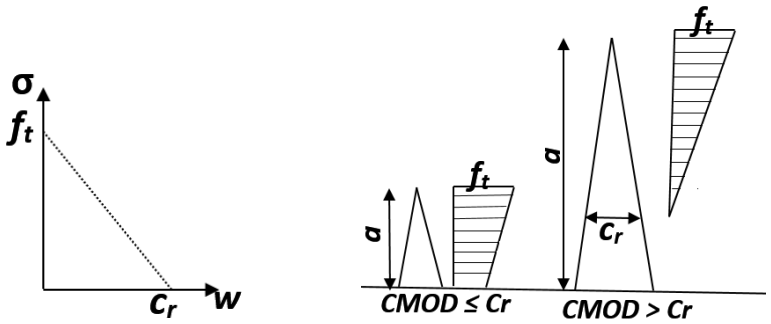

(a) (b)

Figure 1: (a) linear tension softening curve, (b) cohesive tension softening stresses

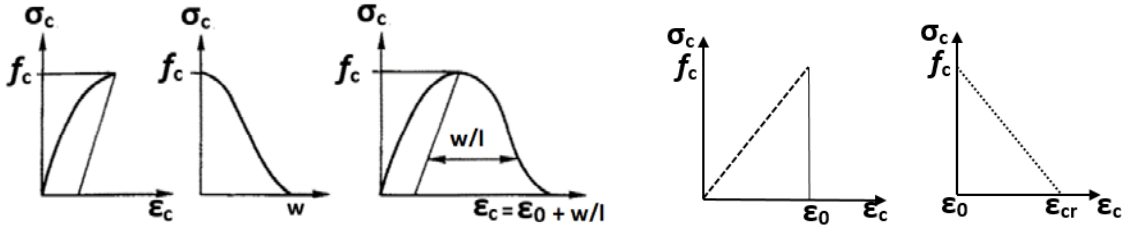

(a) (b)

Figure 2: Compression softening in concrete, (a) stress-strain and stress deformation approach (Hillerborg, 1990) (b) strain softening approach

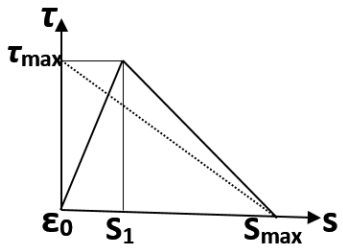

Figure 3: Bi-linear bond-slip model and idealised linear bond-slip

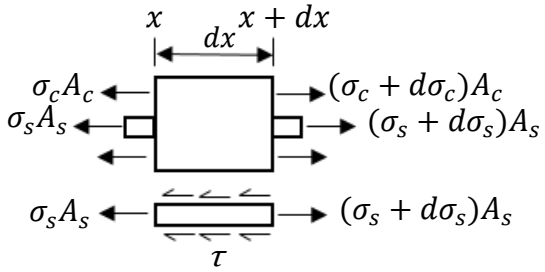

Figure 4: Stresses in an element dx when pulled out in tension

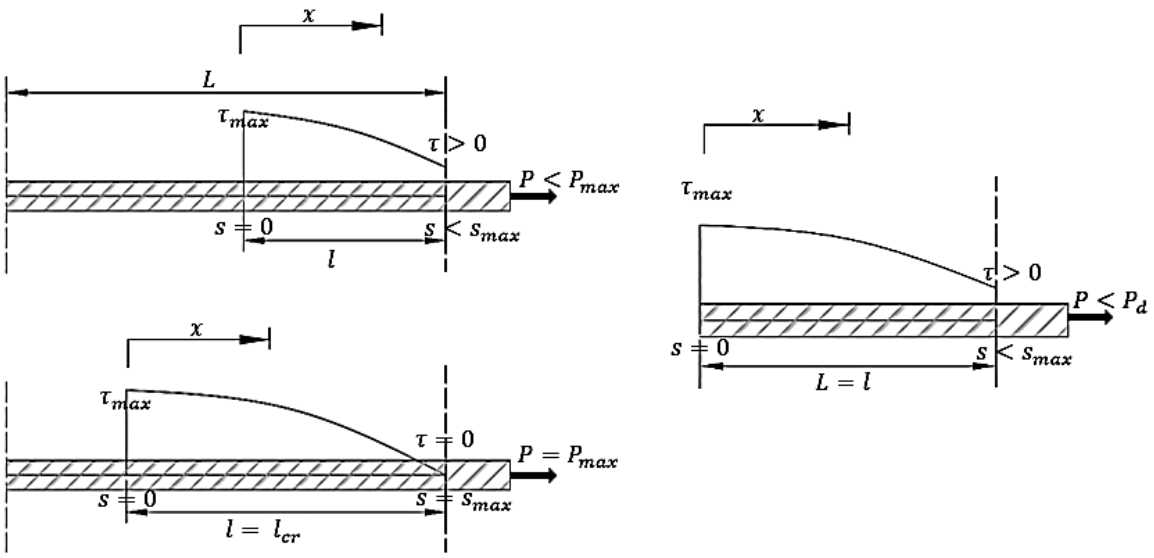

(a) *(b)*

Figure 5: The bond behaviour in pull-out test; (a) when $L \geq l_{cr}$, (b) when $L < l_{cr}$

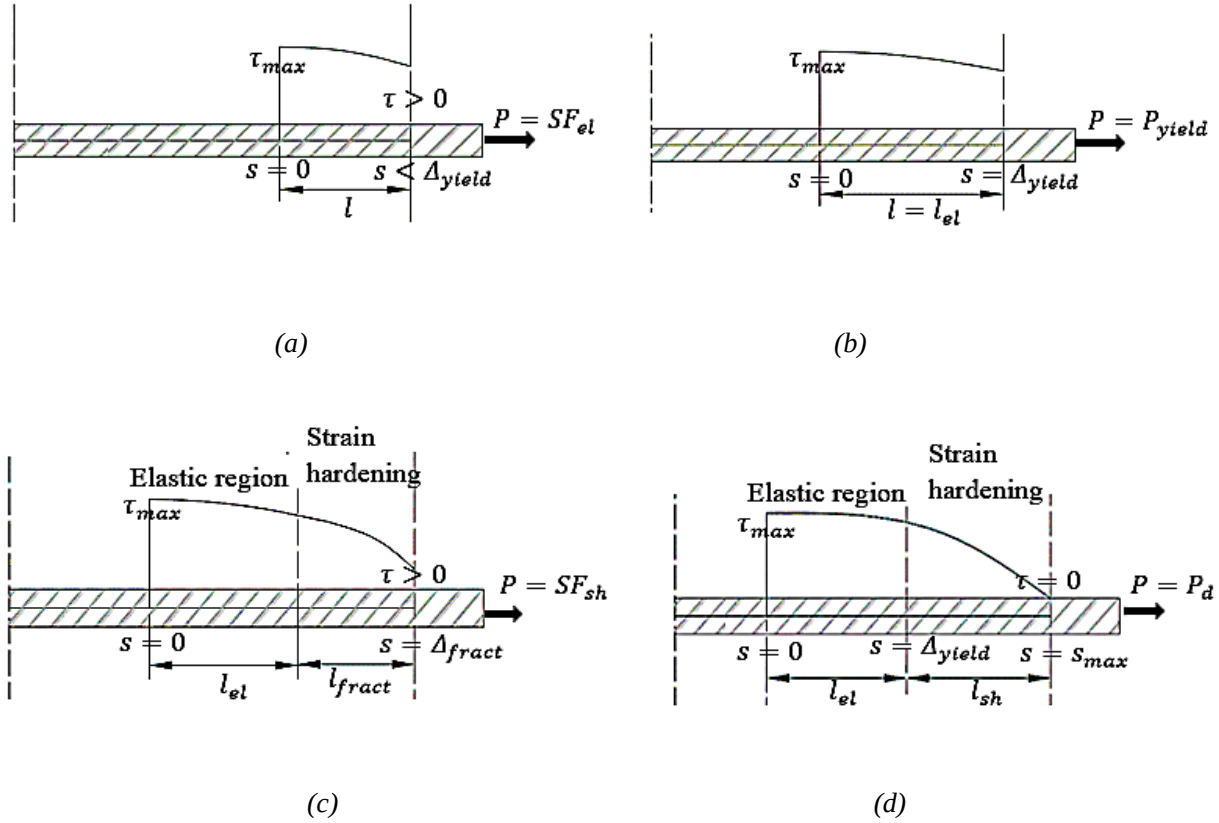

Figure 6: Bond-slip and stress distribution (a) phase 1 - in the elastic region (b) phase 2 - at first yield (c) phase 3 - after yielding when fracture is critical and (d) phase 3 - after yielding when debonding is critical

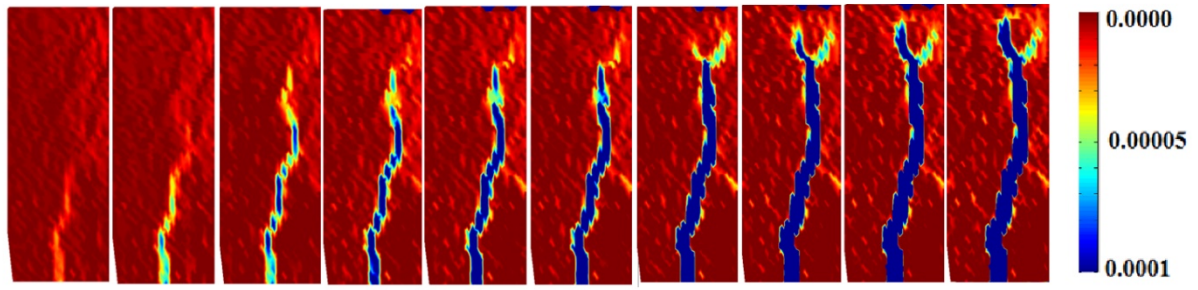

Figure 7: Crack development and strain profile in a lightly reinforced concrete beam [69].

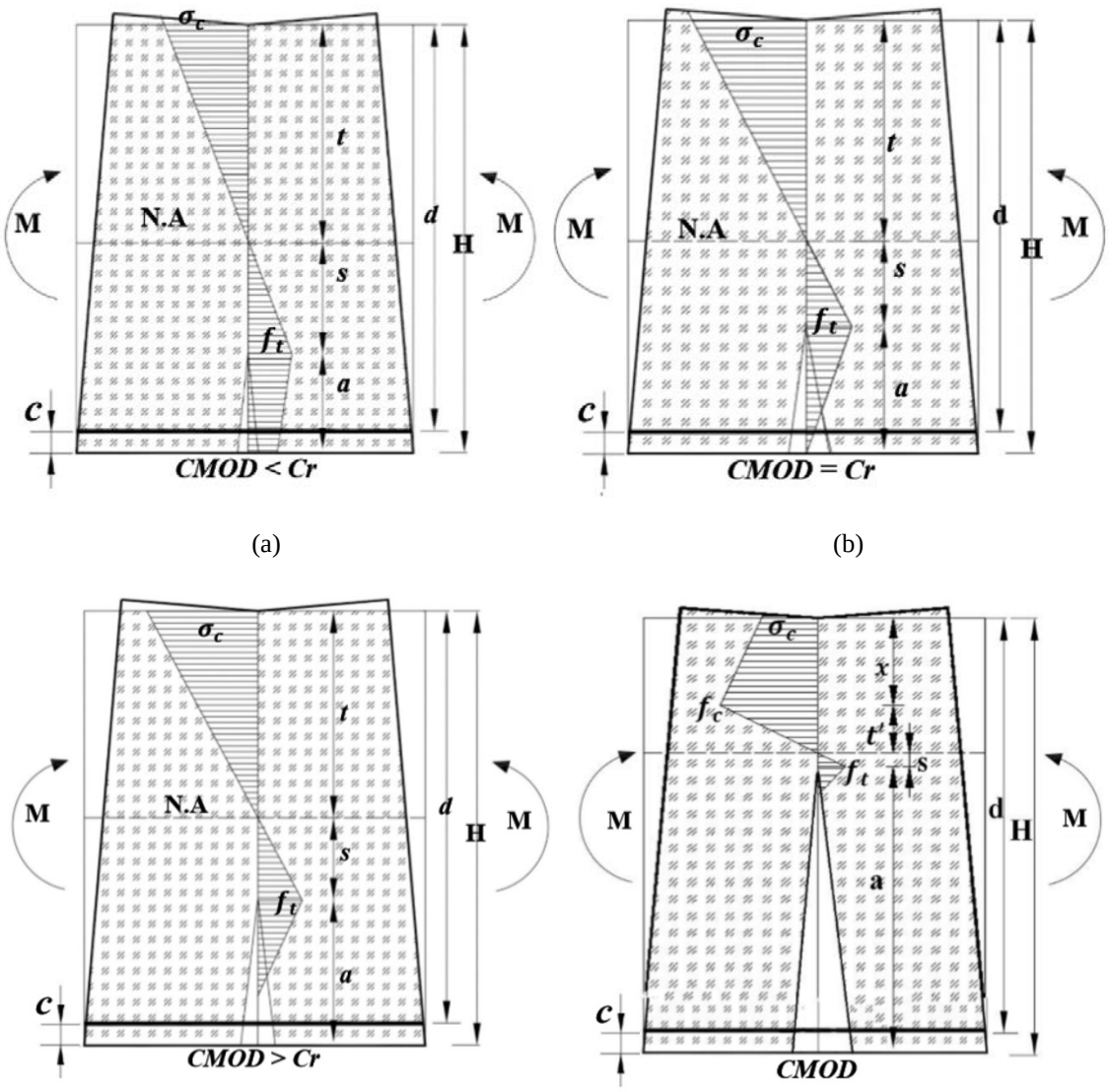

Figure 8: Crack development –(a) Stage I when CMOD < C_r (b) Stage II when CMOD = C_r (c) Stage II when CMOD > C_r and (d) Stage III, crack development

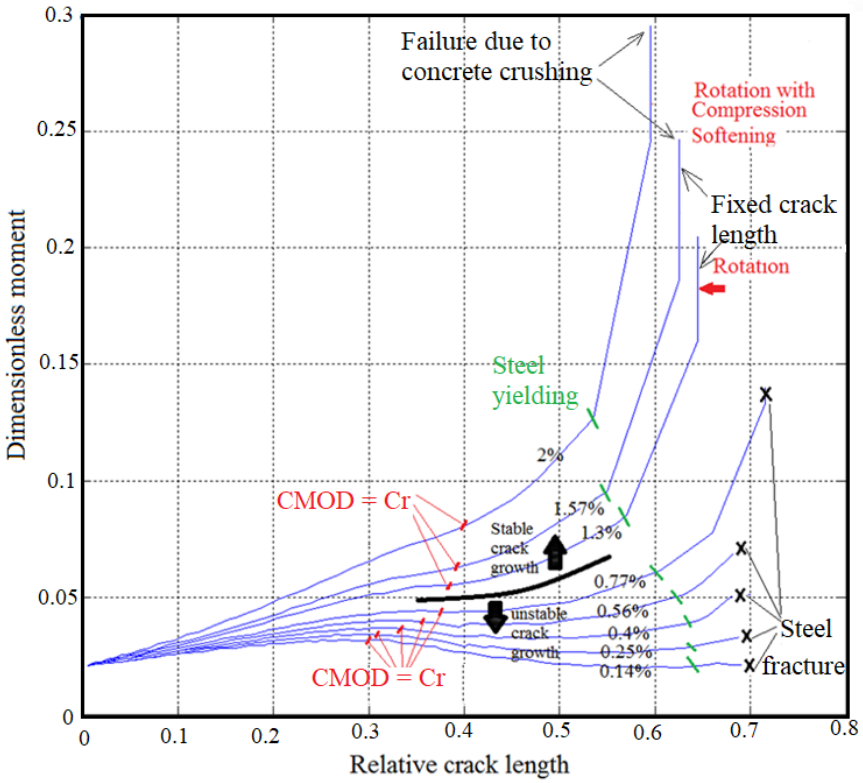

Figure 9: Moment-crack length prediction for RC beams with different reinforcement ratios

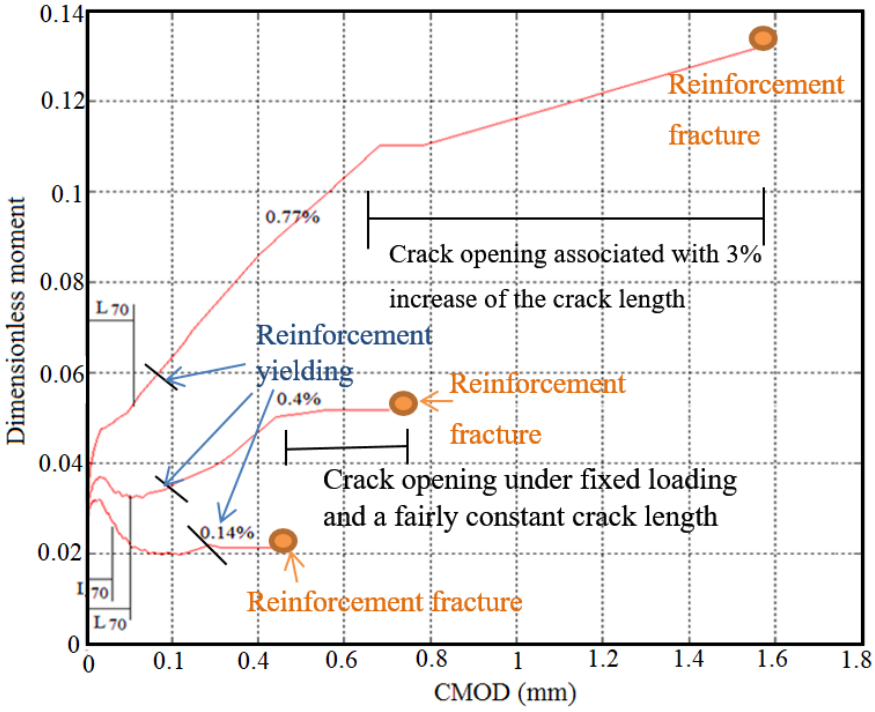

Figure 10: Moment-CMOD prediction for RC beams with different reinforcement ratios

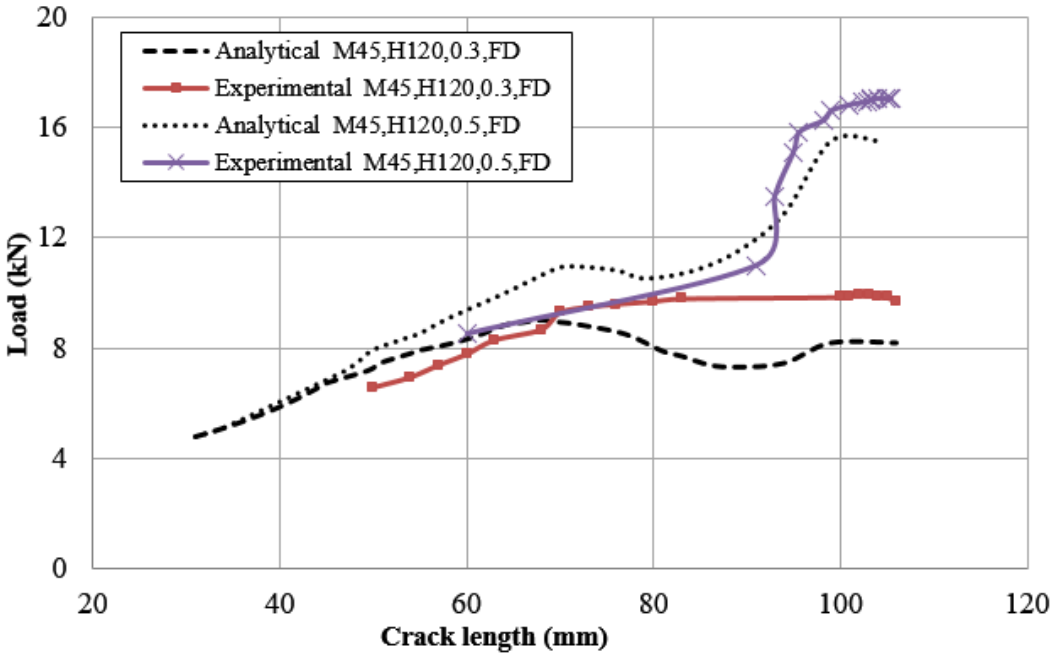

Figure 11: Experimental and predicted behaviour of beams of depth 120mm

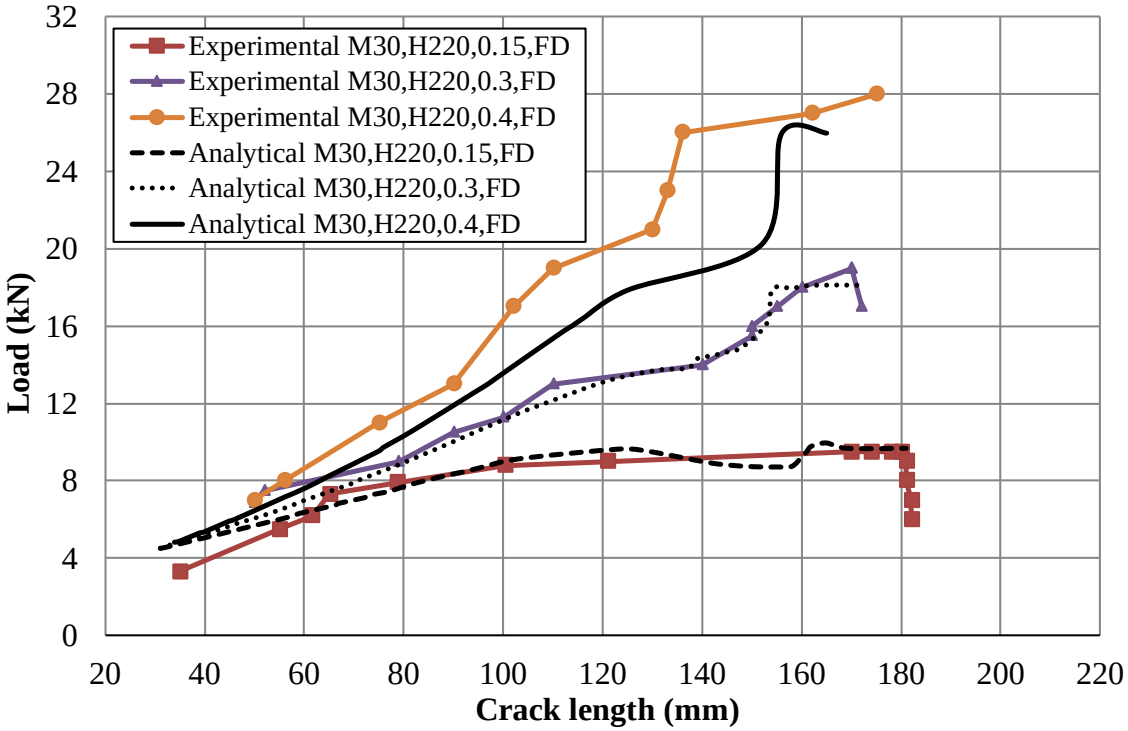

Figure 12: Experimental and predicted behaviour of beams of depth 220mm

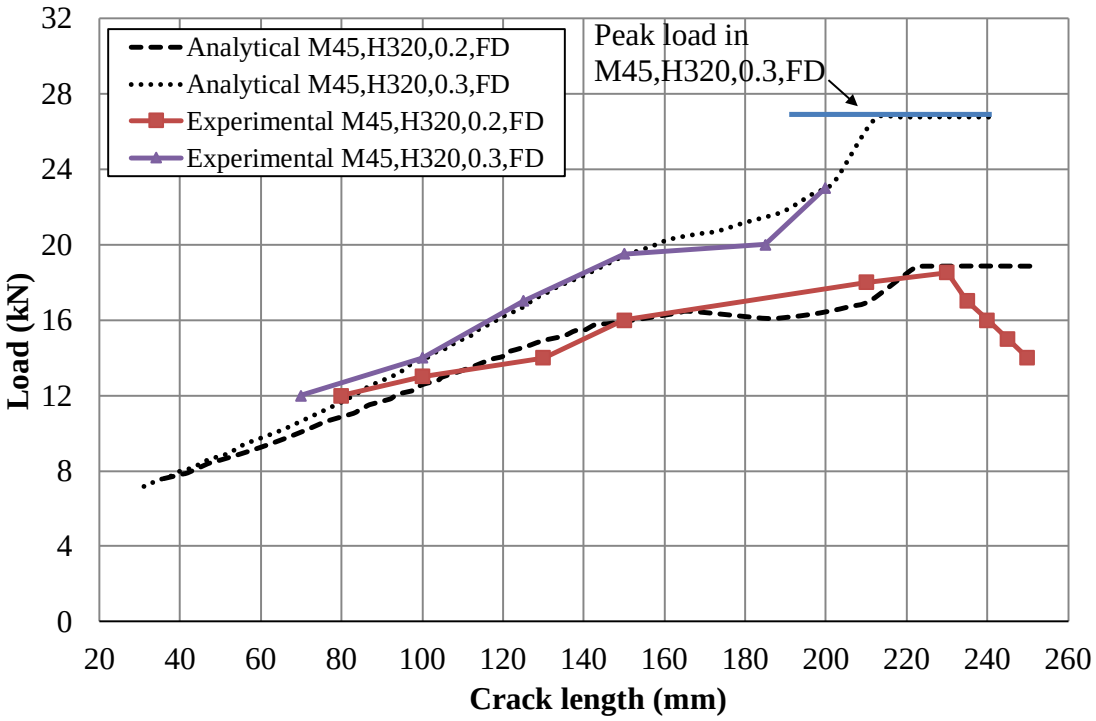

Figure 13: Experimental and predicted behaviour of beams of depth 320 mm

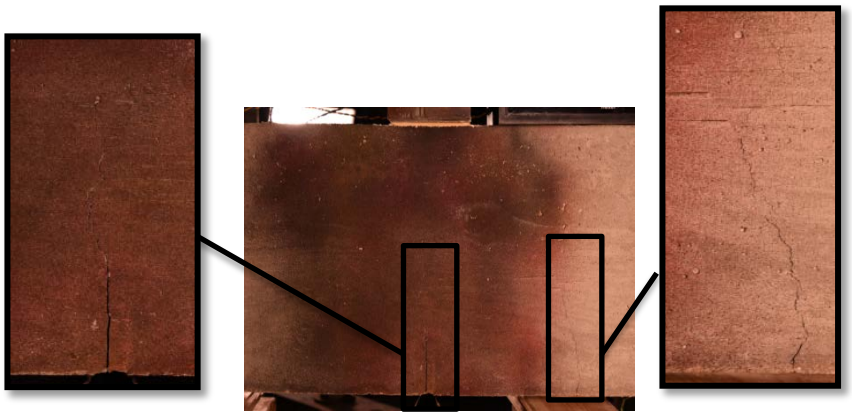

Figure 14: Cracks in beam M30,H220,0.4,FD

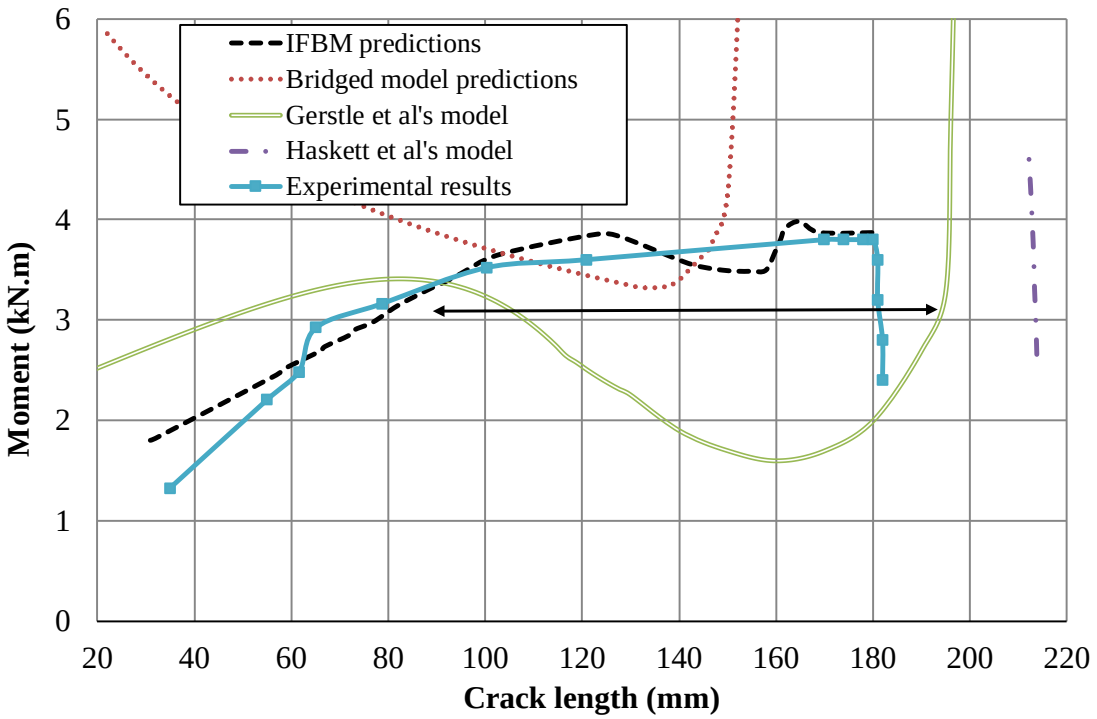

Figure 15: IBFM predictions for beam M30,H220,0.15,FD and comparison with other models